Facet Engineering for Manipulated Photoluminescence Blinking from Perovskite Nanocrystals

Mrinal Kanti Panda,[a] Debopam Acharjee,[a] Asit Baran Mahato,[a] and Subhadip Ghosh[a,b]*

[a]*School of Chemical Sciences, National Institute of Science Education and Research (NISER), An OCC of Homi Bhabha National Institute (HBNI), Khurda 752050 Odisha, India.*

[b]*Center for Interdisciplinary Sciences (CIS), National Institute of Science Education and Research (NISER), An OCC of Homi Bhabha National Institute (HBNI), Khurda 752050, Odisha, India.*

**Email: sghosh@niser.ac.in*

ABSTRACT: Photoluminescence (PL) blinking of nanoparticles, while detrimental for their optoelectronic and imaging applications, can be beneficial for next-generation displays, especially when blinking is precisely controlled by reversible electron/hole injection from an external source. Efforts have been made toward forming a definite charged state to understand trion-induced PL-blinking by electrochemical charging of nanoparticles, which may lead to greater control over PL-blinking. A key parameter deciding the success of controllable PL-blinking from nanoparticles is their affinities towards photo-oxidation and/or photo-reduction. This work shows that facet engineering renders perovskite nanocrystals (PNCs) with distinct blinking properties based on their number of facets. Interestingly, the off-duration (τ_{off}) in the PL intensity time-trace and the fraction time spent in the off-state of a surface-immobilized PNC enhance as the number of facets increases from six (cube-PNC) to twelve (dodecahedron-PNC) and, to twenty-six (rhombicuboctahedron-PNC). Our observation suggests a greater affinity for photo-charging of extra faceted PNCs.

KEYWORDS: *facet engineering, trion, charged exciton, single particle blinking, polyhedral perovskite nanocrystals*

Auger recombination in nanoparticles causes electron-hole recombination by transferring the energy non-radiatively to a third carrier, causing intra-band excitation of the carrier that ultimately relaxes, dissipating excess energy to heat.[1-5] Auger recombination in small nanoparticles, including PNCs, is exceptionally first, not only because of the close proximity of interacting charges but also the momentum conservation relaxation leading to fast dynamics on timescales of a few hundreds of picoseconds (ps) or less.[2, 6-7] Weakly emissive charged excitons or trions are detrimental to the nanoparticles' optoelectronic applications, including lasers, LEDs, and single emission sources; nevertheless, the deliberately occurring trions can benefit next-generation displays. Notably, reported literature shows that the emission from QD-LEDs is largely quenched by the charging of the emitting layer that, in turn, enhances the non-radiative Auger losses within charged particles and limits the external quantum efficiency.[8] Since charging/discharging to nanoparticles is a reversible process, one can think of taking advantage of this property for display applications, possibly by designing a logical imbalance between hole and electron injection rates for the intentional darkening to some pixels on the emitting layer while keeping others emissive.[9-10] Vacha and colleagues could manage to modulate the PL of $CsPbBr_3$ nanocrystal at the single-particle level by applying an external electric field; the field strength decided the extent of charging to the nanocrystals and eventually the PL intensity.[10] However, this idea is not much explored for PNC-display applications, primarily because its implementation requires a rational understanding of several critical parameters, including how the shape-morphology of nanoparticles controls the PL blinking, which is less thoroughly studied for PNCs. We nicely demonstrated here how the PL blinking can be modulated by changing the particle morphology, leading to photo-charging with different extents based on the number of facets.

Recent studies show that, in some cases, electrochemical charge injection can produce a well-defined trion state in nanoparticles, though this task is tedious and challenging. However, photoexcitation can easily create the charged exciton within a nanoparticle but with lesser control. Photoinduced uncompensated charge in nanoparticles, stemming from the trapping (and tunnelling) of the charge carriers by surface trap states (and to a nearby substrate), Auger ionization etc.[4,11-13] Large efforts have been invested to realizing the factors that may help create trion states within a nanoparticle, whereby exploiting these parameters can render greater control over nanoparticle blinking, which is the ultimate goal of the next-generation QD-LED display. So far, several factors that can influence trion with complex trends have been reported, such as particle

morphology, heterostructures, nanoparticle volume, etc.[14-17] For instance, a seminal work by Klimov and colleagues shows that the trion state can be deferred by passivating the core-only QDs by large band gap semiconductor materials epitaxially grown all over the QDs and employing interfacial alloying.[2] A recent report by the same group shows that the trion state with greater control requires both intentional alloying of core-shell QDs and photochemical doping.[18] In this letter, we have demonstrated the easy manipulation of PL-blinking of PNCs by facet engineering. Interestingly, we observed that the propensity for forming a trion state increases with the number of PNC facets.

RESULTS AND DISCUSSION

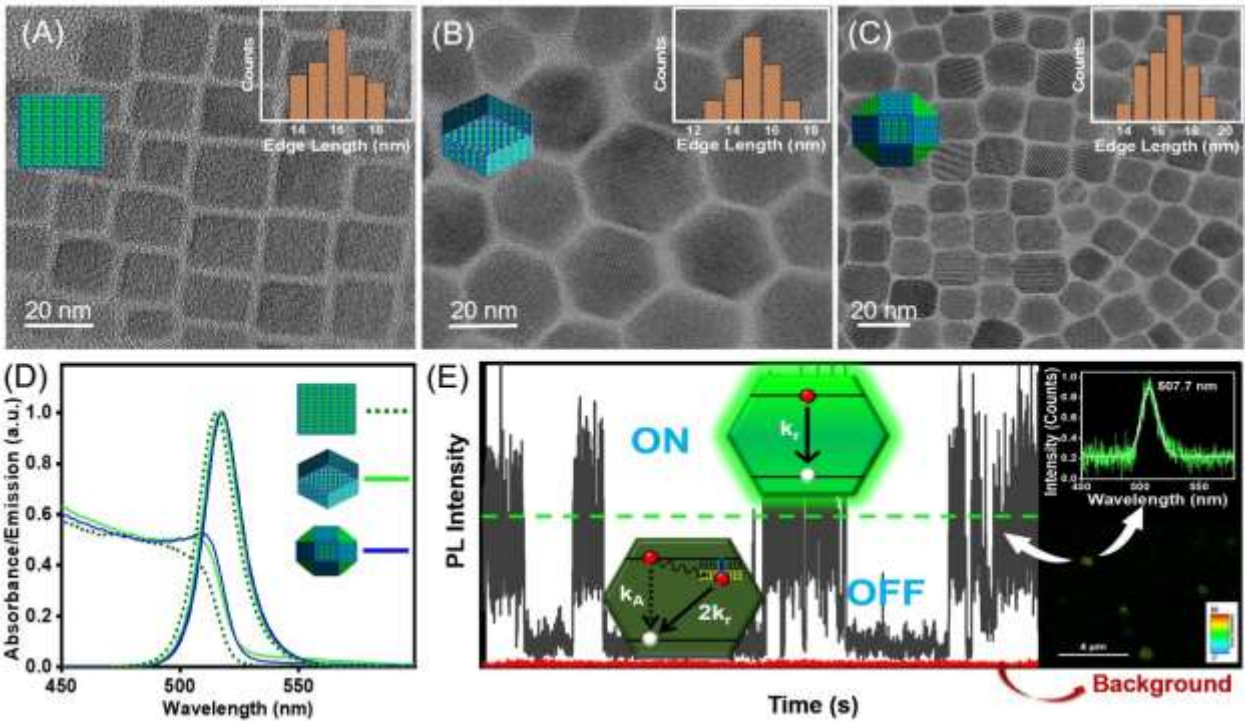

Figure 1. (A-C) HRTEM images of PNCs of different morphologies, six-faceted cube (c-PNC) (A), twelve-faceted dodecahedron (d-PNC) (B), and twenty-six-faceted rhombicuboctahedron (r-PNC) (C). Insets show edge-length distributions. (D) PL and absorption spectra (λ_{ex} ~400 nm) of PNCs dispersed in toluene. (E) Schematics of charge neutral (bright-green) and negatively charged (dark-green) exciton recombination mechanisms in single PNC causing on- and off-states in PL intensity time-trace. The black and yellow horizontal dashed lines within the off-state particle represent the shallow and deep trap states. After recording the PL intensity time-trace, we confirmed from the single-particle spectral signature of PNC (shown on the right) that the recorded PL was from PNC only. 3-D illustrations of particle morphologies in Fig. A-D and later Figs. are reproduced from *Nano Lett.* 2022, *22*, 8908−8916. Copyright 2022 American Chemical Society.

We synthesized three batches of $CsPbBr_3$ PNCs following reported literature with, respectively, six- (cube), twelve- (dodecahedron) and twenty-six (rhombicuboctahedron) facets [See the Supporting Information (SI)].[19-22] Figures 1A-C depict the HRTEM images of PNCs of different morphologies, inset showing their similar average particle sizes (~17±1 nm) and narrow size distributions. We further characterized our PNC sample by XRD (Figure S1), XPS (Figure S2), PL dynamics (Figure S3) and steady-state optical studies (Figure 1D); all results nicely correlate with previous reports.[19-27] Our PNC samples are identical in every aspect, i.e., chemical compositions, particle sizes, photoluminescence quantum yields (PLQYs~78-82%), absorption and PL spectra, etc., except for their number of facets.

Earlier studies with smaller-sized c-PNCs ($CsPbBr_3$) have reported arbitrary PL fluctuations between bright (on), dim (grey) and dark (off) states, referred to as PL-blinking or intermittency, stemming from the participation of surface trap-states in electron-hole recombination process.[28-31] Klimov and co-workers employing a time-tagged, time-correlated single photon counting (TCSPC) measurement of PL-blinking from PNCs ($CsPbBr_3/CsPbI_3$), confirmed that while the bright state is related to recombination of charge neutral excitons, the origin of dark (off) and dim (grey) states lies, respectively, in recombination of positive and negative trions.[2] If a photo-carrier is trapped in a deep trap state for an extended period, PNC becomes charged. The subsequent absorption of the second photon by charged PNC produces trion (dark-green particle in Figure 1E).[2] recombination of trion state may involve both (i) nonradioactive Auger process by transferring recombination energy to the uncompensated carrier, discussed before and (ii) a radiative process with a rate constant twice high (i.e., $2k_r$) compared to radiative recombination rate (k_r) of neutral exciton. The trion state recombination (radiative and non-radiative) causing PL-blinking of nanoparticles is called AC blinking.[3]

For the single-particle PL-blinking study, a highly diluted solution of PNCs in 3% poly(methyl methacrylate) (PMMA) was spin-coated on a coverslip. The low areal density (~0.09 μm^2) of PNC on the coverslip ensured the easy isolation of PNCs by confocal microscope (Figure 1E right lower inset). The single-particle PL time-trace was recorded by exciting at ~422 nm, utilizing a pulse laser (~7 MHz repetition rate, pulse width ~150 ps, power ~0.01 kW/cm^2). Throughout our experiment, we maintained minimal average excitonic occupancy ($\langle N \rangle$ ~0.06), deduced from the relationship $\langle N \rangle$= (photon fluence per pulse) × (absorption cross-section).[32] Typical single-particle PL spectrum of c/d/r-PNC is characterized by a full width at half-

maximums (FWHMs) of ~18±4 nm and peak positions at ~509±3 nm, respectively (right-upper inset of Figure 1E). Typical PL time-traces of the individual c/d/r-PNCs under low excitonic occupancy (<N> ~0.06) are depicted in Figure 2A-C.

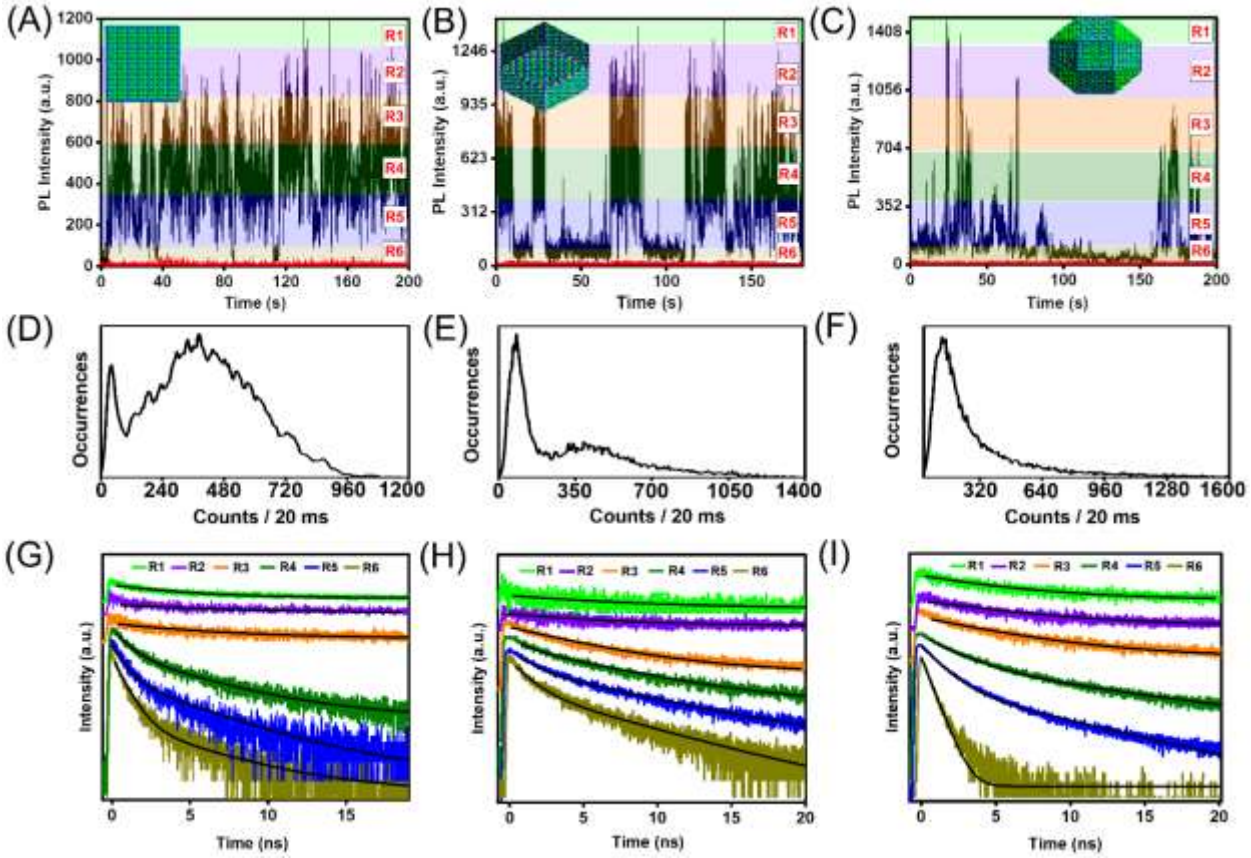

Figure 2. PL time-traces (upper panel, 20 ms binning time) along with occurrence probabilities of different intensity levels (middle panel) and PL dynamics (lower panel) recorded from a single c-PNC (A, D, G), d-PNC (B, E, H) and r-PNC (C, F, I). PL lifetime curves of different intensity states in the lower panel are obtained by collecting emissions from different intensity regions shown by shaded areas (upper panel) with specific colours corresponding to the colours of lifetime curves. Off-state durations in the upper panel increase with an increasing number of facets. Low-intensity states (~40 cts/20 ms) reside much above the background level (~8 cts/20 ms), implying off-states are weakly emissive.

Intensity histograms can resolve PL intensities broadly into two states- (i) bright or on-states described by a much narrower distribution and (ii) dim or off-states with a wide distribution (Figure 2D-F). However, the bimodal feature gradually converted into singly distributed retaining off-states only as the number of facets increases (Figure 2D-F). We assign off-states to trions based on the analyses of PL lifetimes and intensities, and their correlations in fluorescence-lifetime-intensity-distribution (FLID) plots and earlier reports, discussed in the later part of this manuscript.

Figure 2A-C reveals a complex relationship between blinking kinetics and particle morphology: the off-state durations (τ_{off}s) and their occurrence probabilities increase with the

number of facets. The integrity of this observation was further confirmed by repeating the experiment over 120 particles, randomly picking up 40 particles from each morphology (c-, d-, r-PNCs), showing a similar trend (Figure S4). The overall observation implies that increasing the number of facets of PNCs poses a greater risk for photo-charging, rendering off-states prevalent in PL time-trace.

Table 1. Lifetime Components (τ_i) along with Contributions (α_i) of c-/d-/r-PNCs for Different Intensity Regions

sample	region	$\tau_1(\alpha_1)$, ns	$\tau_2(\alpha_2)$, ns
c-PNC / d-PNC / r-PNC	R1	-	9 / 8.6 / 9
	R2	-	7 / 7 /7
	R3	-	5 / 6 / 6
	R4	0.9 (0.73) / 1.1 (0.38) / 1.5 (0.73)	6 (0.27) / 7 (0.62) / 7 (0.27)
	R5	0.8 (0.69) / 1.1 (0.57) / 1.2 (0.88)	5 (0.31) / 7 (0.43) / 7 (0.12)
	R6	0.8 (0.87) / 1.0 (0.93) / 0.8 (1.0)	6 (0.13) / 6 (0.07) / -

The origins of on- and off-states were determined by analyzing the PL dynamics of different intensity levels (Figure 2G-I); for that, we resolved the PL-intensities into six distinct zones marked with, respectively, from R1 (most intense) to R6 (least intense) (Figure 2A-C). Irrespective of morphology, PL dynamics of high-intense regions (R1-R3) are characterized by single lifetime components representing mostly charge-neutral excitonic recombinations (radiative) (Table 1). In contrast, intermediate states (R4-R5) with an additional short lifetime component (~0.8-1.5 ns) suggest the participation of trion recombination (radiative and non-radiative) and contributing more in extra-faceted PNCs. Notably, while the lowest intensity state (R6) of r-PNCs involves trion recombination only (~0.8 ns single component), R6 dynamics of the other two PNCs are governed by both excitonic and trion recombinations (biexponential lifetime components) (Table 1).

We computed the intensity-lifetime scaling (η) for high-intensity regions (R1-to-R3), which readily gives us an idea of radiative recombination rates [$k_r^{Ri(i=1-3)}$] of different intensity regions relative to the R1 (k_r^{R1}), later is normalized to 1.[33]

$\eta = k_r^{R1}(I_1/\tau_1):k_r^{R2}(I_2/\tau_2):k_r^{R3}(I_3/\tau_3)$=1.0:1.0:1.0 (for c-PNCs) and 1.0:1.0:0.90 (for d-PNCs) and 1.0:0.90:0.88 (for r-PNCs)

Where I_i and τ_i are, respectively, the average PL-intensity and lifetime of Ri region. Radiative recombination rates of high-intensity levels (R1-R3) maintain a near unity ratio for all the cases, except for little deviation at R3 level as the facet increases. This observation suggests competition between variable non-radiative rates and fixed radiative rate, the former originating from shallow trap states mediated non-radiative band edge recombination (NBC).[3,28,33] If a charge carrier traps in a shallow trap state (short-lived), it immediately relaxes following a non-radiative process much before a second exciton is created. The carrier trapping rate by shallow trap state fluctuates with time, leading to PL-blinking of nanoparticles, known as NBC blinking.[3,28,33] NBC blinking causes intensity change accompanied by proportionate lifetime change without modifying the radiative rate.

From R3 onward, η value falls from near-unity, suggesting the participation of other competing process(es) along with NBC recombination and, most importantly, contributing more to the low-intensity regions. Further, a short lifetime component (~0.8-1.5 ns) starts evolving at low-intensity regions, whose contribution increases while moving from R4-to-R6 (Table 1). Consulting previous reports and considering our low excitonic occupancy (<N>~ 0.06) deterring from multi-excitonic recombination, we assign ~0.8-1.0 ns lifetime component of R6 to trion recombination, whereas ~9 ns component of R1 to excitonic recombination (Table 1).[33] NBC recombination is prominent in R1-R3, and trion precedes over NBC in R4-R6.

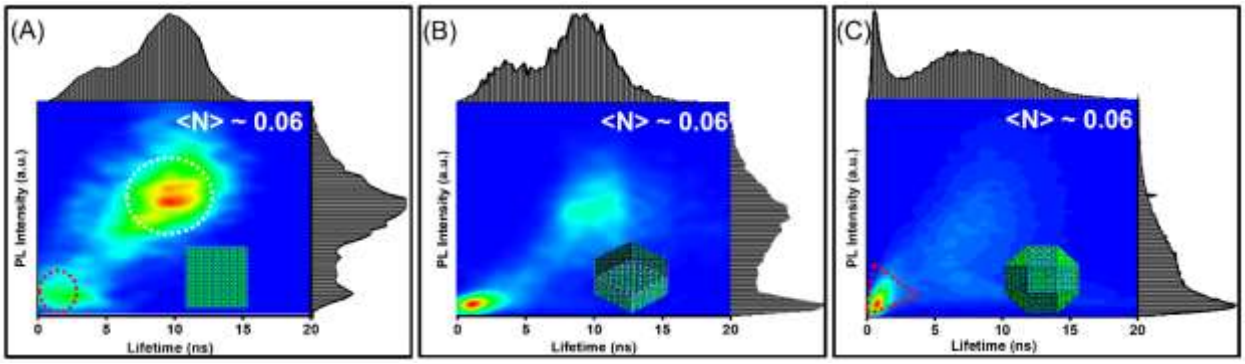

Figure 3. FLID of single (A) c-PNC, (B) d-PNC and (C) r-PNC, obtained by the correlating intensity and lifetime histograms shown in the top (along the x-axis) and right side (along the y-axis) of the plots. False colour changing from red to blue implies a decreasing occurrence probability of a given state in FLID space. The red triangle in Fig. C shows the trion state.

Notably, the contribution of the trion component of any of the low-intensity regions (R4/R5/R6) increases with increasing number of facets, since the extra faceted PNCs are more vulnerable to photo-charging (Table 1). This assertion is also prominent in the FLID plots, showing that although the overall PL-blinking of PNC involves NBC and trion recombinations, the latter's occurrence probability drastically increases in extra-faceted r-PNC (Figure 3A-C).[3] In the present case, occurrences of on- (circled in white, ~ 9 ns) and off- (circled in red, ~1 ns) states are equally probable in the FLID plot of c-PNC (Figure 3A). However, the on-state population reduces and then obliterates as we move from c-PNC to r-PNC through d-PNC, clearly due to the larger involvement of trion states in extra faceted PNCs (Figure 3). Trajectory describing the occurrence probability of on-states with long lifetimes (circled in white) is related to NBC recombination, while trajectory relating off-states with low intensities (circled in red) is persuasive to trion recombination.[1,3,33] Trion is more prominent in the FLID of r-PNC where the off-state trajectory maintains a steeper slope because of a higher radiative rate; Mulvaney and colleagues reported a similar observation in the FLID of CdSe-based QD.[3] The lifetimes of the trion state of similar PNCs were reported to be ~0.78-0.94 ns, nicely correlating with our value (Table 1).[1,33]

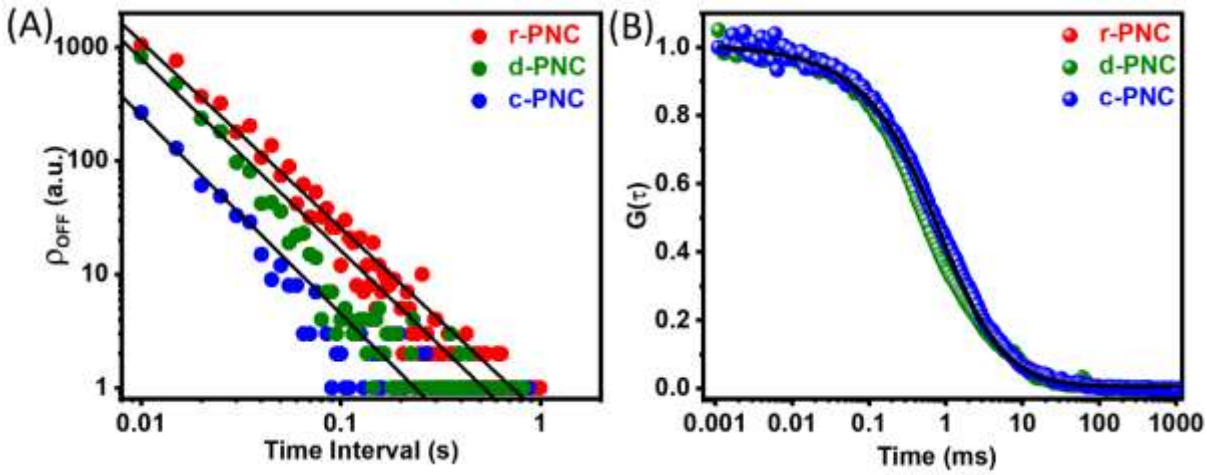

Figure 4. (A) Probability density distribution of off-state durations of PNCs with different morphologies. (B) FCS curves (normalized to initial time) of the same three PNCs dispersed in toluene show identical blinking and diffusion kinetics (λ_{ex}~422 nm, power ~0.03 kW/cm^2).

We further investigated the occurrence probabilities of off-states from the PL time-traces of all three PNCs (Figure 4A); showing their decay kinetics are inverse power-law distributed.[4, 28, 35] Intensity levels underneath a threshold mark placed in the middle of average on- and off-state intensities (green dashed line in Figure 1E), 5 ms binning time and a long statistical sample time

(~250 s) were considered while calculating the off-state probability density function [$\rho(\tau_{off})$ s^{-1}] (Figure 4A). Although the shortest τ_{off} is limited by binning time (~5 ms), the longest off time can be comparable to the data acquisition time. With the help of SymPhoTime 64 software, τ_{off}s with different durations and their occurrence probabilities are determined for all three PNCs and then plotted in a histogram (log-log representation), showing the occurrence probabilities of off-durations increase with increasing the number of facets (Figure 4A). Also, the probability density of longer τ_{off} (> 0.1 s) states is considerably higher in extra-faced PNCs, possibly due to the greater extent of photo-charging. Furthermore, the inverse power-law behaviour of probability density plots, i.e., $\rho(\tau_{off}) \alpha \tau_{off}^{-m}$, is consistent with the literature.[4, 28, 35] The value of the power-law exponent (m) ranges from ~ 1.64-1.75, which is also consistent with earlier reports showing similar values over six orders of magnitude of τ_{off}.[28]

Next, we performed a fluorescence correlation spectroscopy (FCS) study of the blinking kinetics of all three PNCs in the solution phase (dispersed in toluene) (Figure 4B).[36-42] The FCS autocorrelation curves fit nicely to the following analytical equation, considering blinking stemming from (i) dispersive trap states, which is an intrinsic property of the PNCs, and (ii) three-dimensional diffusion, largely dependent on solvent diffusion parameters (Equation 1).[33] Best-fitted parameters are collected in Table 2.

$$G(\tau) = \frac{1}{<N>}\left(1 + \left(\frac{T}{1-T}\right)\exp\left[-\left(\frac{\tau}{\tau_T}\right)^{\beta}\right]\right)\left(1+\frac{\tau}{\tau_D}\right)^{-1}\left(1+\frac{\tau}{\kappa^2\tau_D}\right)^{-1/2} \quad (1)$$

Where τ_T and τ_D are the trap state and diffusion-induced blinking timescales of the PNCs, T is the trap-state fraction, and N is the average number of PNCs undergoing reversible blinking within the excitation volume whose longitudinal-to-transverse radii ratio is represented by κ. β ($0 \leq \beta \leq 1$) is the stretching exponent related to the energy distribution of the trap states.[33]

Table 2. Best-fitted FCS Parameters of c-/d-/r-PNCs

sample	τ_T (μs)	T	β	τ_D(ms)
c-PNC /d-PNC /r-PNC	260/250/255	0.25/0.26/0.24	0.65/0.65/0.65	1/1.01/1

Table 2 reports a few noteworthy observations of the FCS study: (i) τ_D, related to the particle size by the Stokes-Einstein equation, shows near identical values (~1 ms) of all three PNCs, implying their similar hydrodynamic radii.[41-42] (ii) Relatively less off-state fractions (T ~0.25) across the

PNC samples suggest PNCs mostly remain in the on-state in solution phase irrespective of their morphologies, contrasting the solid-state study. (iii) High β values (~0.65) and similar τ_Ts (~250 μs) of all three particles indicate that PL blinking in the solution phase is less dispersive and persuasive to a single non-radiative recombination phenomenon, presumably NBC type. (iv) Per-particle brightness (PPB) observed during the FCS study is found to be similar (~12±2 K cps/particle) for particles with different morphologies, signifying their near identical PLQYs. All these observations unanimously confirm the absence of a trion state in the solution phase, rendering identical PL properties to all three particles from every aspect. Since PNCs quickly leave the excitation volume by diffusion in the solution phase FCS study, photo-charging to PNCs is unlikely. In such a scenario, only NBC recombination can participate in the blinking process involving shallow surface defects adjacent to the conduction band whose origin lies in halogen vacancy and the presence of lead (uncoordinated or nanoparticle).

On the contrary, surface-immobilized PNCs can easily form a trion state due to prolonged excitation to the same particle. Although one can limit NBC recombination in PNCs to its lowest by adopting superior surface passivation methods, rendering PNCs devoid of detects, the extent of trion recombination, however, also depends on the PNC's propensity for photo-charging, which must be related to the particle morphology.[24,31,43-48] Due to prolonged photoexcitation, trion recombination takes precedence over NBC in PL-blinking of surface-immobilized PNC.[3] An optically pumped surface immobilized PNC can quickly form a trion state by transferring either of the charge carriers to adjacent material. The greater the number of facets of the PNC, the larger would be the probability of creating a trion state. Multi-faceted PNCs render efficient binding with adjacent charge scavenger materials/molecules, leading to fast excited state charge transfer.

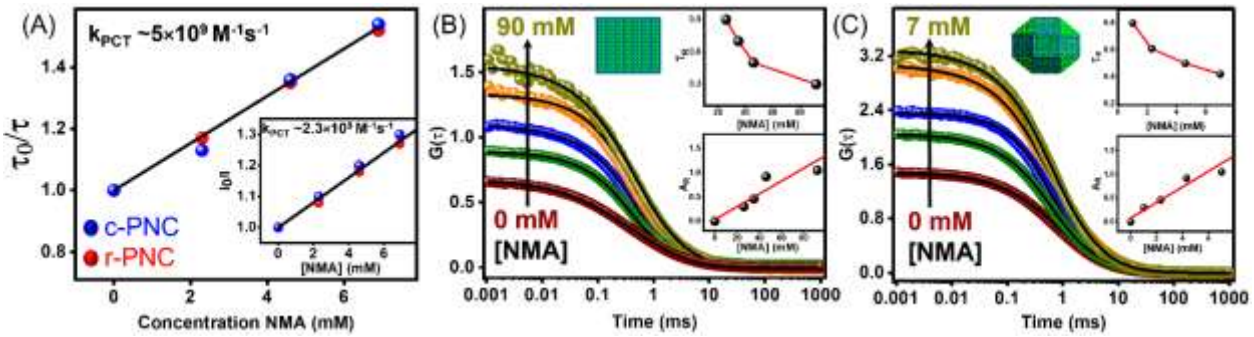

Figure 5. (A) Lifetime and steady-state (inset) Stern-Volmer plots of quenching of PL c-PNC (red balls) and r-PNC (blue balls) by NMA. Quenching rates (k_{PCT}) are similar for both the morphologies and reach close to diffusion-controlled rate. See Figure S5 for the lifetime and steady-state quenching data of c-/r-PNCs. (B-C) FCS curves of c-PNC (B) and r-PNC (C) at different NMA concentrations. A much steeper slope of "A_R vs. [NMA]" plot (inset) of r-PNC-NMA suggests higher binding affinity of extra-faceted PNCs.

To supplement this assertion, we studied bimolecular photoinduced charge transfer (PCT) kinetics in N-Methylaniline (NMA)-PNC couples of different morphologies in toluene.[49-55] Solvent diffusion hinders solution phase bimolecular PCT studies, where the observed dynamics are mostly diffusion-controlled.[52,56-58] In our case also the Stern-Volmer plots reveal the PCT kinetics are diffusion controlled (k_{PCT} ~5×10^9 $M^{-1}s^{-1}$), which restricted us from deducing the intrinsic PCT timescales of PNC-NMA using a TCSPC set-up (IRF ~90 ps) (Figure 5A). Otherwise, comparing PCT timescales of different morphologies would have immediately confirmed the greater propensity of extra-facted PNCs for photo-charging. Nevertheless, an FCS study asserts that extra-faced PNCs can easily form complexes with quenchers due to the more available binding sites of the extra-faceted PNCs.[59-64] Intuitively, this, in turn, would render a greater probability of PCT creating a trion state in extra-faceted PNC. Likewise, carrier trapping/de-trapping and PNC diffusing into and out of the excitation volume, causing PL-blinking in the FCS study, binding/unbinding of quencher (NMA here) with PNC can also cause similar blinking with timescale essentially different from the timescales (τ_T and τ_D) of other two phenomena (trapping and diffusion). FCS curves of PNCs in the presence of NMA fit nicely to the following equation (Figure 5B-C), which includes one additional term to Equation 1, as follows-

$$G(\tau) = \frac{1}{<N>}\left(1 + A_R \exp\left[-\left(\frac{\tau}{\tau_R}\right)\right]\right)\left(1 + \left(\frac{T}{1-T}\right)\exp\left[-\left(\frac{\tau}{\tau_T}\right)^{\beta}\right]\right)\left(1 + \frac{\tau}{\tau_D}\right)^{-1}\left(1 + \frac{\tau}{\kappa^2\tau_D}\right)^{-1/2} \quad (2)$$

Where τ_R is the dynamical timescale PNC-NMA complexation reaction, and A_R is the amplitude of the binding reaction. Here, we focus primarily on binding reaction parameters (A_R, τ_R) that provide some idea of the binding affinities of PNCs with quenchers based on their morphologies. The equilibrium constant (K) of PNC-NMA was deduced from the relationship $A_R = K[NMA]_0$, assuming the PLQY of the PNC-NMA complex is ~0, and the binding reaction is a pseudo-first-order.[23,59] Much higher magnitude of K and faster τ_R (at similar quencher concentration) of r-PNC-NMA compared to ones of c-PNC-NMA suggest greater binding affinity of the extra-facted PNCs with NMA or other charge-scavenging molecules/materials, and that might be the reason of prolonged off-states in PL time-traces of extra-facted PNCs (Table 3). Thermodynamic consideration of HOMO-LUMO of NMA vis-à-vis VB-CB of PNC suggests photoinduced electron transfer (PET) from HOMO of NMA to the VB of an optically pumped PNC causing the

quenching.[65-67] With an increase in the number of facets in PNC, PET, leading to negatively charged PNC continues to become more efficient.

Table 3. Best-fitted FCS Parameters Related to c-PNC (and r-PNC)-NMA Complexation Reaction. All Other Parameters are Identical to Reported Ones in Table 2.

sample	[NMA] (mM)	A_R	K(M^{-1})	τ_R(μM)
c-PNC /r-PNC	0/0	-	100/300	-
	26/1	2.6/0.3		0.9/0.8
	35/2.3	3.5/0.46		0.7/0.61
	46/4.6	4.6/0.92		0.5/0.5
	90/7	9.2/1.05		0.4/0.42

CONCLUSION

We demonstrated here how surface engineering renders PNCs with different blinking properties based on their morphologies. Since photo-charging provides no control over creating a trion state in PNC of one type (positive or negative), we can't firmly confirm the charge of the trion state participating in the blinking here. However, comparing off-state lifetime with reported ones for similar systems suggests the participation of negative trion is of greater possibility in the recombination process of our PNCs.[2] Blinking in the solution phase, while mostly ruled by NBC recombination across the morphologies, in surface-immobilized state trion recombination takes precedence over NBC and the latter being largely dependent on particle morphology, allowing surface engineering to modulate the blinking property through varying the number of facets. This work highlights the massive potential of facet engineering in next-generation display applications.

METHODS

Synthesis of c-/d-/r PNCs

Syntheses of c-/d-/r-PNCs followed the reported procedures in our previous publication.[22] High-temperature sample drying under an inert environment was considered in almost every steps. In brief, first, we prepared Cesium-oleate by heating the required amounts of Cs_2CO_3, oleic acid (OA) and octadecene (ODE) at ~130 ^{0}C for ~60 mins in the N_2 environment. Obtained Cesium-oleate was preheated to >100 ^{0}C, before using it in the next steps.

Next, required amounts of PbO, phenacyl bromide, oleic acid (OA), Oleylamine (OAm), and ODE were mixed together and heated to a temperature of ~130 ^{0}C under an inert atmosphere. A red-coloured reaction mixture was obtained and then the temperature was increased further to >200 ^{0}C. After prolonged heating (~ 1 hr), ~0.5 ml Cs-oleate (prepared in the first step) was quickly added to the reaction mixture. Then the reaction was quenched in an ice bath after 20 mins of annealing. The obtained d-PNC sample was purified through repeated centrifugations in a solvent mixture; details of this synthesis can be found elsewhere.[22]

r-PNC (and c-PNC) sample was synthesized following an identical procedure of d-PNC synthesis, except for the annealing time, here it is ~45 mins (~1 min). The rest of the steps/parameters are quite similar to d-PNC synthesis, apart from few slight modifications, reported elsewhere.[22]

Single-Particle Measurement PL time-traces and FCS study were performed in MT-200 confocal microscope from PicoQuant. While FCS study uses 60x water immersion objective, PL time-trace recording utilizes a 100x oil objective with a high numerical aperture. Two single-photon avalanche photodiode (SPAD) detectors and 50/50 beam splitter directing emission to two SPADs were used in FCS study to avoid after-pulse effects in the FCS curves. A long-pass filter blocking ~422 nm laser and 50 μm diameter pinhole were placed in the emission path. FCS study was performed by diluting the PNC sample in toluene to <1 nM concentration. A few drops of diluted sample were placed on a coverslip and subsequently sealed in a special sample chamber for FCS measurement. On the other hand, a surface-immobilized PNC sample was prepared by spin coating extremely diluted PMMA solution of PNC (few pM PNC in 3% PMMA) on a coverslip. We enabled time-tagged time-resolved mode while recording PL time-traces that allowed us for FLID and other lifetime-related plots and analyses using SymPhoTime software. Excitonic occupancy per pulse per PNC was calculated from the equation <N>=(per-pulse photon fluence)×(absorption cross-section). Absorption cross-section value (~2×10^{-14} cm^2)[68] was obtained from the literature for similar excitation wavelength and extrapolating the value for PNC of size ~17 nm.

ASSOCIATED CONTENT

Supporting Information
The Supporting Information is available free of charge on the ACS Publications website at DOI: xx.xxxx/acsnano.xxxxxxx.

XRD spectra (S1), XPS spectra (S2), PL dynamics (S3), additional PL blinking time-traces (S4), and steady-state and lifetime quenching data (S5).

AUTHOR INFORMATION

Corresponding Author

Subhadip Ghosh−*School of Chemical Sciences, National Institute of Science Education and Research*

And

Center for Interdisciplinary Sciences (CIS), National Institute of Science Education and Research(NISER), An OCC of Homi Bhabha National Institute (HBNI), Khurda 752050 Odisha, India; orcid.org/0000-0002-8527 5534;

Email: sghosh@niser.ac.in

Authors

Mrinal Kanti Panda−*School of Chemical Sciences, National Institute of Science Education and Research, An OCC of Homi Bhabha National Institute(HBNI), Khurda 752050 Odisha, India*

Debopam Acharjee−*School of Chemical Sciences, National Institute of Science Education and Research, An OCC of Homi Bhabha National Institute(HBNI), Khurda 752050 Odisha, India*

Asit Baran Mahato−*School of Chemical Sciences, National Institute of Science Education and Research, An OCC of Homi Bhabha National Institute(HBNI), Khurda 752050 Odisha, India*

REFERENCES

1. Park, Y.-S.; Guo, S.; Makarov, N. S.; Klimov, V. I. Room Temperature Single-Photon Emission from Individual Perovskite Quantum Dots. *ACS Nano* **2015**, *9*, 10386−10393.
2. Park, Y. S.; Bae, W. K.; Pietryga, J. M.; Klimov, V. I. Auger Recombination of Biexcitons and Negative and Positive Trions in Individual Quantum Dots. *ACS Nano* **2014**, *8*, 7288−7296.
3. Yuan, G.; Gómez, D. E.; Kirkwood, N.; Boldt, K.; Mulvaney, P. Two Mechanisms Determine Quantum Dot Blinking. *ACS Nano* **2018**, *12*, 3397−3405.
4. Peterson, J. J.; Nesbitt, D. J. Modified Power Law Behavior in Quantum Dot Blinking: A Novel Role for Biexcitons and Auger Ionization. *Nano Lett.* **2009**, *9*, 338−345.
5. Li, Q.; Yang, Y.; Que, W.; Lian, T. Size- and Morphology-Dependent Auger Recombination in $CsPbBr_3$ Perovskite Two-Dimensional Nanoplatelets and One-Dimensional Nanorods. *Nano Lett.* **2019**, *19*, 5620−5627.
6. Aneesh, J.; Swarnkar, A.; Kumar Ravi, V.; Sharma, R.; Nag, A.; Adarsh, K. V. Ultrafast Exciton Dynamics in Colloidal $CsPbBr_3$ Perovskite Nanocrystals: Biexciton Effect and Auger Recombination. *J. Phys. Chem. C* **2017**, *121*, 4734−4739.

7. Eperon, G. E.; Jedlicka, E.; Ginger, D. S. Biexciton Auger Recombination Differs in Hybrid and Inorganic Halide Perovskite Quantum Dots. *J. Phys. Chem. Lett.* **2018**, *9*, 104−109.
8. Bae, W. K.; Park, Y.-S.; Lim, J.; Lee, D.; Padilha, L. A.; McDaniel, H.; Robel, I.; Lee, C.; Pietryga, J. M.; Klimov, V. I. Controlling the Influence of Auger Recombination on the Performance of Quantum-Dot Light-Emitting Diodes. *Nat. Commun.* **2013**, *4*, 2661.
9. Schindler, F.; Lupton, J. M.; Mueller, J.; Feldmann, J.; Scherf, U. How Single Conjugated Polymer Molecules Respond to Electric Fields. *Nat. Mater.* **2006**, *5*, 141–146.
10. Sharma, D. K.; Hirata, S.; Biju, V.; Vacha, M. Stark Effect and Environment-Induced Modulation of Emission in Single Halide Perovskite Nanocrystals. *ACS Nano* **2019**, *13*, 624–632.
11. Klimov, V. I.; McBranch, D. W. Auger-Process-Induced Charge Separation in Semiconductor Nanocrystals. *Phys. Rev. B* **1997**, *55*, 13173–13179.
12. Krauss, T. D.; Brus, L. E. Charge, Polarizability, and Photoionization of Single Semiconductor Nanocrystals. *Phys. Rev. Lett.* **1999**, *83*, 4840–4843.
13. Li, S.; Steigerwald, M. L.; Brus, L. E. Surface States in the Photoionization of High-Quality CdSe Core/Shell Nanocrystals. *ACS Nano* **2009**, *3*, 1267–1273.
14. Zhao, J.; Nair, G.; Fisher, B. R.; Bawendi, M. G. Challenge to the Charging Model of Semiconductor-Nanocrystal Fluorescence Intermittency from Off-State Quantum Yields and Multiexciton Blinking. *Phys. Rev. Lett.* **2010**, *104*, 157403.
15. Zavelani-Rossi, M.; Lupo, M. G.; Tassone, F.; Manna, L.; Lanzani, G. Suppression of Biexciton Auger Recombination in CdSe/CdS Dot/Rods: Role of the Electronic Structure in the Carrier Dynamics. *Nano Lett.* **2010**, *10*, 3142–3150.
16. Oron, D.; Kazes, M.; Banin, U. Multiexcitons in Type-II Colloidal Semiconductor Quantum Dots. *Phys. Rev. B* **2007**, *75*, 035330.
17. García-Santamaría, F.; Chen, Y.; Vela, J.; Schaller, R. D.; Hollingsworth, J. A.; Klimov, V. I. Suppressed Auger Recombination in "Giant" Nanocrystals Boosts Optical Gain Performance. *Nano Lett.* **2009**, *9*, 3482–3488.
18. Wu, K.; Lim, J.; Klimov, V. I. Superposition Principle in Auger Recombination of Charged and Neutral Multicarrier States in Semiconductor Quantum Dots. *ACS Nano* **2017**, *11*, 8437–8447.

19. Bera, S.; Behera, R. K.; Pradhan, N. *α*-Halo Ketone for Polyhedral Perovskite Nanocrystals: Evolutions, Shape Conversions, Ligand Chemistry, and Self-Assembly. *J. Am. Chem. Soc.* **2020**, *142*, 20865−20874.
20. Bera, S. K.; Bera, S.; Shrivastava, M.; Pradhan, N.; Adarsh, K. V. Facet Engineering for Amplified Spontaneous Emission in Metal Halide Perovskite Nanocrystals. *Nano Lett.* **2022**, *22*, 8908−8916.
21. Justice Babu, K.; Kaur, G.; Shukla, A.; Saha, R.; Kaur, A.; Sachdeva, M.; Yadav, D. K.; Ghosh, H. N. Fast Polaron Formation and Low Carrier Mobility in Defect-Free Polyhedral $CsPbBr_3$ Perovskite Nanocrystals. *ACS Photonics* **2022**, *9*, 969−978.
22. Acharjee, D.; Das, A.; Panda, M. K.; Barai, M.; Ghosh, S. Facet Engineering for Decelerated Carrier Cooling in Polyhedral Perovskite Nanocrystals. *Nano Lett.* **2023**, *23*, 1946-1953.
23. Das, A.; Acharjee, D.; Panda, M. K.; Mahato, A. B.; Ghosh, S. Dodecahedron $CsPbBr_3$ Perovskite Nanocrystals Enable Facile Harvesting of Hot Electrons and Holes. *J. Phys. Chem. Lett*. **2023**, *14*, 3953-3960.
24. Mahankudo, S. K.; Das, A.; Mishra, K.; Barai, M.; Mal, P.; Ghosh, S. Synthesis of Cs/Methylammonium/Formamidinium $PbBr_3$ Perovskite Nanocrystals with Green Emissions: Implications for Display Applications. *ACS Appl. Nano Mater.* **2022**, *5*, 4360−4366.
25. Manna, A.; Dinda, T. K.; Ghosh, S.; Mal, P. $CsPbBr_3$ in the Activation of the C−Br Bond of $CBrX_3$(X = Cl, Br) under Sunlight. *Chem. Mater.* **2023**, *35*, 628−637.
26. Mishra, K.; Acharjee, D.; Das, A.; Ghosh, S. Femtosecond Upconversion Study of Interfacial Electron Transfer from Photo-excited $CsPbBr_3$ Perovskite Nanocrystal to Rhodamine 6G. *J. Phys. Chem. B* **2021**, *125*, 11017−11025.
27. Sayyad, U. S.; Burai, S.; Bhatt, H.; Ghosh, H. N.; Mondal, S. Efficient Charge Transfer in the Perovskite Quantum Dot–Hemin Biocomposite: Is This Effective for Optoelectronic Applications? *J. Phys. Chem. Lett.* **2023**, *14*, 5397–5402.
28. Cordones, A. A.; Leone, S. R. Mechanisms for Charge Trapping in Single Semiconductor Nanocrystals Probed by Fluorescence Blinking. *Chem. Soc. Rev.* **2013**, *42*, 3209−3221.

29. Paul, S.; Kishore. G; Samanta, A. Photoluminescence Blinking of Quantum Confined $CsPbBr_3$ Perovskite Nanocrystals: Influence of Size. *J. Phys. Chem. C* **2023**, *127*, 10207–10214.
30. Garai, A.; E. Krishnan Vishnu; Banerjee, S.; Nair, A. A.; Bera, S.; K. George Thomas; Pradhan, N. Vertex-Oriented Cube-Connected Pattern in $CsPbBr_3$ Perovskite Nanorods and Their Optical Properties: An Ensemble to Single-Particle Study. *J. Am. Chem. Soc.* **2023**, *145*, 13989–13999.
31. Dey, A.; Ye, J. Z.; De, A.; Debroye, E.; Ha, S. K.; Bladt, E.; Kshirsagar, A. S.; Wang, Z. Y.; Yin, J.; Wang, Y.; Quan, L. N.; Yan, F.; Gao, M. Y.; Li, X. M.; Shamsi, J.; Debnath, T.; Cao, M. H.; Scheel, M. A.; Kumar, S.; Steele, J. A.; et al. State of the Art and Prospects for Halide Perovskite Nanocrystals. *ACS Nano* **2021**, *15*, 10775−10981.
32. Makarov, N. S.; Guo, S.; Isaienko, O.; Liu, W.; Robel, I.; Klimov,V. I. Spectral and Dynamical Properties of Single Excitons, Biexcitons, and Trions in Cesium-Lead-Halide Perovskite Quantum Dots. *Nano Lett.* **2016**, *16*, 2349−2362.
33. Ahmed, T.; Seth, S.; Samanta, A. Mechanistic Investigation of the Defect Activity Contributing to the Photoluminescence Blinking of $CsPbBr_3$ Perovskite Nanocrystals. *ACS Nano* **2019**, *13*, 13537−13544.
34. Chen, J.; Messing, M. E.; Zheng, K.; Pullerits, T. Cation-Dependent Hot Carrier Cooling in Halide Perovskite Nanocrystals. *J. Am. Chem. Soc.* **2019**, *141*, 3532−3540.
35. Verberk, R.; van Oijen, A. M.; Orrit, M. Simple Model for the Power-Law Blinking of Single Semiconductor Nanocrystals. *Phys. Rev.B: Condens. Matter Mater. Phys.* **2002**, *66*, 233202.
36. Dey, S.; Mandal, U.; Adhikari, A.; Ghosh, S.; Bhattacharyya, K. Probing Dynamic Heterogeneity in Nanoconfined Systems: The Femtosecond Excitation Wavelength Dependence and Fluorescence Correlation Spectroscopy. *Hydrog. Bond. Transfer Excit. State* **2010**, *1*, 159−174.
37. Koley, S.; Ghosh, S. Encapsulation and Residency of a Hydrophobic Dye within the Water-Filled Interior of a PAMAM Dendrimer Molecule. *J. Phys. Chem. B* **2017**, *121*, 1930−1940.

38. Das, A.; Mishra, K.; Ghosh, S. Revealing Explicit Microsecond Carrier Diffusion from One Emission Center to Another in an All-Inorganic Perovskite Nanocrystal. *J. Phys. Chem. Lett.* **2021**, *12*, 5413−5422.
39. Mishra, K.; Das, A.; Ghosh, S. Subpicosecond Charge Separation Time Scale at Graphene Quantum Dot Surface. *J. Phys. Chem. C* **2020**, *124*, 24115−24125.
40. Kundu, S.; Das, S.; Patra, A. Fluorescence Correlation Spectroscopy and Fluorescence Lifetime Imaging Microscopy for Deciphering the Morphological Evolution of Supramolecular Self-Assembly. *Chem. Comm.* **2023**, *59*, 8017–8031.
41. Ghosh, S.; Mandal, U.; Adhikari, A.; Bhattacharyya, K. Study of Diffusion of Organic Dyes in a Triblock Copolymer Micelle and Gel by Fluorescence Correlation Spectroscopy. *Chem. Asian J.* **2009**, *4*, 948−954.
42. Haustein, E.; Schwille, P. Fluorescence correlation spectroscopy: Novel variations of an established technique. *Annu. Rev. Biophys. Biomol. Struct.* **2007**, *36*, 151−169.
43. Zhang, Y.; Siegler, T. D.; Thomas, C. J.; Abney, M. K.; Shah, T.; DeGorostiza, A.; Greene, R. M.; Korgel, B. A. A "Tips and Tricks" Practical Guide to the Synthesis of Metal Halide Perovskite Nanocrystals. *Chem. Mater.* **2020**, *32*, 5410−5423.
44. Bohn, B. J.; Tong, Y.; Gramlich, M.; Lai, M. L.; Döblinger, M.;Wang, K.; Hoye, R. L. Z.; Müller-Buschbaum, P.; Stranks, S. D.;Urban, A. S.; Polavarapu, L.; Feldmann, J. Boosting Tunable BlueLuminescence of Halide Perovskite Nanoplatelets through Post-synthetic Surface Trap Repair. *Nano Lett.* **2018**, *18*, 5231−5238.
45. Wu, Y.; Wei, C.; Li, X.; Li, Y.; Qiu, S.; Shen, W.; Cai, B.; Sun,Z.; Yang, D.; Deng, Z.; Zeng, H. In Situ Passivation of PbBr64−Octahedra toward Blue Luminescent $CsPbBr_3$ Nanoplatelets with Near 100% Absolute Quantum Yield. *ACS Energy Lett.* **2018**, *3*, 2030−2037.
46. Imran, M.; Caligiuri, V.; Wang, M.; Goldoni, L.; Prato, M.; Krahne, R.; De Trizio, L.; Manna, L. Benzoyl Halides as Alternative Precursors for the Colloidal Synthesis of Lead-Based Halide Perovskite Nanocrystals. *J. Am. Chem. Soc.* **2018**, *140*, 2656−2664.
47. Liu, P.; Chen, W.; Wang, W.; Xu, B.; Wu, D.; Hao, J.; Cao, W.; Fang, F.; Li, Y.; Zeng, Y.; Pan, R.; Chen, S.; Cao, W.; Sun, X. W.; Wang, K. Halide-Rich Synthesized Cesium Lead Bromide Perovskite Nanocrystals for Light-Emitting Diodes with Improved Performance. *Chem. Mater.* **2017**, *29*, 5168−5173.

48. Otero-Martínez, C.; Garcia-Lojo, D.; Pastoriza-Santos, I.; Perez-Juste, J.; Polavarapu, L. Dimensionality Control of Inorganicand Hybrid Perovskite Nanocrystals by Reaction Temperature: From No-Confinement to 3D and 1D Quantum Confinement. *Angew. Chem., Int. Ed.* **2021**, *60*, 26677−26684.
49. Mishra, K.; Acharjee, D.; Das, A.; Ghosh, S. Subpicosecond Hot Hole Transfer in a Graphene Quantum Dot Composite with High Efficiency. *J. Phys. Chem. Lett.* **2022**, *13*, 606−613.
50. Bharadwaj, K.; Choudhary, H.; Hazra, S.; Ghosh, S. Study of Interfacial Charge Transfer from an Electron Rich Organic Molecule to CdTe Quantum Dot by Using Stern-Volmer and Stochastic Kinetic Models. *ChemPhysChem* **2020**, *21*, 415– 422.
51. Bharadwaj, K.; Choudhary, H.; Hazra, S.; Ghosh, S. Role of Emissiveand Non-Emissive Complex Formations in Photoinduced Electron Transfer Reaction of CdTe Quantum Dots. *Chem.- AsianJ.* **2019**, *14*, 4207−4216.
52. Koley, S.; Panda, M. R.; Ghosh, S. Study of Diffusion-Assisted Bimolecular Electron Transfer Reactions: CdSe/ZnS Core-Shell Quantum Dot Acts as an Efficient Electron Donor and Acceptor. *J. Phys. Chem. C* **2016**, *120*, 13456−13465.
53. Mondal, S.; Ghosh, S.; Sahu, K.; Sen, P.; Bhattacharyya, K.Excited-State Proton Transfer from Pyranine to Acetate in Methanol. *Proc. - Indian Acad. Sci., Chem. Sci*.**2007**, *119*, 71−76.
54. Mandal, U.; Ghosh, S.; Dey, S.; Adhikari, A.; Bhattacharyya, K. Ultrafast Photoinduced Electron Transfer in the Micelle and the Gel Phase of a PEO-PPO-PEO Triblock Copolymer. *J. Chem. Phys.* **2008**, *128*, 164505−164510.
55. Koley, S.; Ghosh, S. The Study of Electron Transfer Reactions in a Dendrimeric Assembly: Proper Utilization of Dendrimer Fluorescence. *Phys. Chem. Chem. Phys.* **2016**, *18*, 24830−24834.
56. Koch, M.; Rosspeintner, A.; Angulo, G.; Vauthey, E. Bimolecular Photoinduced Electron Transfer in Imidazolium-Based Room-Temperature Ionic Liquids Is Not Faster than in Conventional Solvents. *J. Am. Chem. Soc.* **2012**, *134*, 3729– 3736.
57. Mukherjee, P.; Das, A.; Sengupta, A.; Sen, P. Bimolecular Photoinduced Electron Transfer in Static Quenching Regime: Illustration of Marcus Inversion in Micelle. *J. Phys. Chem. B* **2017**, *121*, 1610−1622.

58. Kumbhakar, M.; Manna, A.; Sayed, M.; Kumar, A.; Pal, H. Observation of the Marcus Inverted Region for Bimolecular Photoinduced Electron-Transfer Reactions in Viscous Media. *J. Phys. Chem. B* **2014**, *118*, 10704−10715.
59. Al-Soufi, W.; Reija, B.; Novo, M.; Felekyan, S.; Kühnemuth, R.; Seidel, C. A. M. Fluorescence Correlation Spectroscopy, a Tool to Investigate Supramolecuar Dynamics: Inclusion Complexes of Pyronines with Cyclodextrin. *J. Am. Chem. Soc.* **2005**, *127*, 8775−8784.
60. Sharma, S.; Pal, N.; Chowdhury, P. K.; Sen, S.; Ganguli, A. K. Understanding Growth Kinetics of Nanorods in Microemulsion: A Combined Fluorescence Correlation Spectroscopy, Dynamic Light Scattering, and Electron Microscopy Study. *J. Am. Chem. Soc.* **2012**, *134*, 19677−19684.
61. Clovis, N. S.; Sen, S. G-Tetrad-Selective Ligand Binding Kinetics in G-Quadruplex DNA Probed with Fluorescence Correlation Spectroscopy. *J. Phys. Chem. B* **2022**, *126*, 6007−6015.
62. Singha, P.K.; Kistwal, T; Datta, A. Single-Particle Dynamics of ZnS Shelling Induced Replenishment of Carrier Diffusion for Individual Emission Centers in $CuInS_2$ Quantum Dots. *J. Phys. Chem. Lett.* **2023**, *14*, 4289–4296.
63. Ghosh, S.; Adhikari, A.; Sen Mojumdar, S.; Bhattacharyya, K. A Fluorescence Correlation Spectroscopy Study of the Diffusion of an Organic Dye in the Gel Phase and Fluid Phase of a Single Lipid Vesicle. *J. Phys. Chem. B* **2010**, *114*, 5736−5741.
64. Zhang, X.; Poniewierski, A.; Sozański, K.; Zhou, Y.; Brzozowska-Elliott, A.; Holyst, R. Fluorescence correlation spectroscopy for multiple-site equilibrium binding: a case of doxorubicin–DNA interaction. *Phys. Chem. Chem. Phys.* **2019**, *21*, 1572– 1577.
65. Ravi, V. K.; Markad, G. B.; Nag, A. Band Edge Energies and Excitonic Transition Probabilities of Colloidal $CsPbX_3$ (X = Cl, Br, I) Perovskite Nanocrystals. *ACS Energy Lett.* **2016**, *1*, 665– 671.
66. Bhowmik, A.; Kaur, H.; Koley, S.; Jana, S.; Ghosh, S. Diffusion Assisted Bimolecular Electron Injection to CdS Quantum Dots: Existence of Different Regimes in Time Dependent Sink Term of Collins-Kimball Model. *J. Phys. Chem. C* **2016**, *120*, 5308−5314.

67. Jonsson, M.; Wayner, D. D. M.; Lusztyk, J. Redox and Acidity Properties of Alkyl and Arylamine Radical Cations and the Corresponding Aminyl Radicals. *J. Phys. Chem. A* **1996**, *100*, 17539−17543.
68. Castañeda, J. A.; Nagamine, G.; Yassitepe, E.; Bonato, L. G.;Voznyy, O.; Hoogland, S.; Nogueira, A. F.; Sargent, E. H.; Cruz, C. H.; Padilha, L. A. Efficient Biexciton Interactionin Perovskite Quantum Dotsunder Weakand Strong Confinement. *ACS Nano* **2016**,*10*, 8603−8609.

TOC